Single-cell RNA sequencing reveals melanoma cell state-dependent heterogeneity of response to MAPK inhibitors

Su Yin Lim,[a,b,*] Yingxin Lin,[c,d] Jenny H. Lee,[a,b,e] Bernadette Pedersen,[a,b] Ashleigh Stewart,[a,b] Richard A. Scolyer,[b,d,f,h] Georgina V. Long,[b,d,g,h] Jean Y. H. Yang,[c,d] and Helen Rizos[a,b]

[a]Macquarie Medical School, Faculty of Medicine, Health and Human Sciences, Macquarie University, Australia
[b]Melanoma Institute Australia, Australia
[c]School of Mathematics and Statistics, The University of Sydney, Australia
[d]Charles Perkins Centre, The University of Sydney, Australia
[e]Department of Neurosurgery, Chris O'Brien Lifehouse, Sydney, NSW, Australia
[f]Tissue Pathology and Diagnostic Oncology, Royal Prince Alfred Hospital and NSW Health Pathology, Sydney, Australia
[g]Royal North Shore and Mater Hospitals, Sydney, Australia
[h]Faculty of Medicine and Health, The University of Sydney, Australia

eBioMedicine
2024;107: 105308
Published Online xxx
https://doi.org/10.1016/j.ebiom.2024.105308

Summary

Background Melanoma is a heterogeneous cancer influenced by the plasticity of melanoma cells and their dynamic adaptations to microenvironmental cues. Melanoma cells transition between well-defined transcriptional cell states that impact treatment response and resistance.

Methods In this study, we applied single-cell RNA sequencing to interrogate the molecular features of immunotherapy-naive and immunotherapy-resistant melanoma tumours in response to *ex vivo* BRAF/MEK inhibitor treatment.

Findings We confirm the presence of four distinct melanoma cell states - melanocytic, transitory, neural-crest like and undifferentiated, and identify enrichment of neural crest-like and undifferentiated melanoma cells in immunotherapy-resistant tumours. Furthermore, we introduce an integrated computational approach to identify subsets of responding and nonresponding melanoma cells within the transcriptional cell states.

Interpretation Nonresponding melanoma cells are identified in all transcriptional cell states and are predisposed to BRAF/MEK inhibitor resistance due to pro-inflammatory IL6 and TNFα signalling. Our study provides a framework to study treatment response within distinct melanoma cell states and indicate that tumour-intrinsic pro-inflammatory signalling contributes to BRAF/MEK inhibitor resistance.

Funding This work was supported by Macquarie University, Melanoma Institute Australia, and the National Health and Medical Research Council of Australia (NHMRC; grant 2012860, 2028055).

Keywords: Dedifferentiation; Immunotherapy resistance; Computational biology; MAPK inhibitor resistance

Introduction

The overall survival rate of patients with advanced melanoma has tripled to over 50% in the last 10 years as a result of molecular and immune checkpoint inhibitors.[1,2] Almost 70% of patients with $BRAF^{V600}$-mutant melanoma will respond to combination BRAF and MEK molecular inhibitors but less than 20% will have durable responses lasting longer than five years.[3] Immune checkpoint inhibitors targeting CTLA-4 and PD-1 result in 5-year survival rates of 26% and 44%, respectively, while the combination of CTLA-4 and PD-1 inhibitors results in a 5-year survival rate of 52%.[4] Unfortunately, 20–30% of patients responding to PD-1 inhibitors will develop resistance and progress within 1–2 years.[5]

Response and resistance to treatment are influenced by the heterogeneity and plasticity of melanoma cells, which can transition between several phenotypic states. For instance, the transcriptionally-defined undifferentiated and neural crest-like states reflective of

*Corresponding author. Macquarie Medical School, Faculty of Medicine, Health and Human Sciences, Macquarie University, Australia.
E-mail address: esther.lim@mq.edu.au (S.Y. Lim).

Research in context

Evidence before this study

Despite effective molecular and immune-based therapies for patients with advanced melanoma, treatment resistance remains a common and intractable challenge. Treatment resistance is partly driven by the heterogeneity and plasticity of melanoma cells to transition between differentiated and dedifferentiated phenotypic states. However, the precise response and role of melanoma cell states in treatment outcomes remain complex and incompletely understood.

Added value of this study

We dissected the impact of melanoma states in response to molecular therapies using single-cell RNA sequencing of *ex vivo*-treated patient-matched tumour biopsies coupled with a unique single-cell computational biology approach. We show that melanoma dedifferentiation does not determine resistance to BRAF/MEK inhibitors, but rather, tumour-intrinsic pro-inflammatory IL6 and TNFα signalling confer BRAF/MEK inhibitor resistance. Our study provides a valuable framework to delineate molecular mechanisms underlying heterogeneity in treatment response and identify therapeutic targets and biomarkers for treatment resistance.

Implications of all the available evidence

Our finding that dedifferentiated melanoma cells are not inherently resistant to treatment, but rather, are predisposed to BRAF/MEK inhibitor resistance due to pro-inflammatory signalling, represents a conceptual advance and highlights pro-inflammatory pathways as promising targets for combination treatment. Indeed, several ongoing and planned clinical trials (NCT05034536, NCT04652258) are investigating the safety and efficacy of anti-TNFα and anti-IL6 in combination with clinical therapies for melanoma.

dedifferentiated melanoma[6] are more resistant to BRAF/MEK inhibitors[7] and immune-based therapies[8,9] compared to differentiated melanoma. Single-cell sequencing analyses of melanoma biopsies confirmed the co-existence of distinct differentiated and dedifferentiated melanoma cells within primary and metastatic melanoma tumours. These cell states can be identified by the expression of MITF and AXL and their proportions may be influenced by therapy. For instance, $MITF^{low}/AXL^{high}$ dedifferentiated melanoma cells are enriched in melanoma tumours after BRAF/MEK inhibitor therapy,[10] indicating dynamic adaptation and rapid selection of resistant phenotypes in response to treatment. Despite significant advances in single-cell RNA sequencing, there have been few studies utilizing tumour dissociates to examine treatment-induced effects at the single-cell level. As such, the precise response and role of each melanoma cell state in treatment outcomes have yet to be fully elucidated.

In this study, $BRAF^{V600}$-mutant melanoma tissue dissociates derived from tumour biopsies of treatment-naive patients (n = 5) and patients who had progressed on immune checkpoint inhibitors (n = 5) were treated *ex vivo* with combination BRAF/MEK inhibitors dabrafenib and trametinib, and single-cell RNA sequencing (scRNAseq) was used to dissect the molecular features of response in differentiated and dedifferentiated melanoma cells within the same tumour lesion. Discrete melanoma cell states were identified and scored in each tumour biopsy, and an integrated computational approach revealed their unique transcriptomic responses to BRAF/MEK inhibitors. Significantly, we now report that dedifferentiated melanoma cells are not inherently resistant to BRAF/MEK inhibitors, but rather are prone to resistance as a result of intrinsic pro-inflammatory signalling. Our study confirms that melanoma-intrinsic pro-inflammatory IL6 and TNFα signalling confer BRAF/MEK inhibitor resistance and provides a framework to study tumour heterogeneity in treatment response.

Methods

Patient and sample selection

A total of ten patients with advanced metastatic cutaneous melanoma were included in this study. Patients were selected based on availability of tumour samples; fresh tumour biopsies were collected from patients with melanoma following surgical resection. Tumour biopsies were mechanically and enzymatically processed and dissociated into single-cell suspensions using the Tumour Dissociation Kit (Miltenyi Biotec, Australia, Cat no: 130-095-929) and gentleMACS Octo Dissociator (Miltenyi Biotec, Cat no: 130-096-427), according to the manufacturer's instructions. Single-cell tumour suspensions were frozen in 10% dimethyl sulfoxide (DMSO) in human male AB serum (Sigma, St. Louis, MO, USA). Tumour dissociates were initially screened by flow cytometry using Live/Dead NIR and antibodies to detect CD45 and SOX10 (Supplementary Table S1). The following criteria were required for downstream single-cell transcriptome sequencing: >40% viability and >50% tumour content. Patients with melanoma with suitable tumour dissociates were included in the study.

Of the ten patients, five had progressive disease while on treatment with immunotherapy (nivolumab 3 mg/kg every 2 weeks or nivolumab 1 mg/kg plus ipilimumab 3 mg/kg every 3 weeks for four doses followed by nivolumab 3 mg/kg every 2 weeks) while five patients were treatment naive, from the Melanoma Institute Australia (MIA) and Westmead Hospital. Written consent was obtained from all patients (Human Research ethics approval from Royal Prince Alfred

Hospital–Protocol ×15-0454 & HREC/11/RPAH/444). Patient demographics and clinicopathologic features including age, sex, BRAF mutation status, prior treatments and disease distribution were collected. Sex was self-reported by study participants.

Flow cytometric profiling of tumour dissociates

Tumour dissociates were thawed into TIL media (Roswell Park Memorial Institute-1640 media supplemented with 10% heat-inactivated human serum (Sigma), 2 mM glutamine (Gibco, Thermo Fisher Scientific, Waltham, MA, USA), 25 mM HEPES (Gibco), 100 U/ml penicillin and 0.1 mg/ml streptomycin (Gibco) and 50 μg/ml gentamicin (Sigma)), washed and viable cells enriched using the Dead Cell Removal kit (Miltenyi Biotec, Cat no: 130-090-101) and MS columns (Miltenyi Biotec, Cat no: 130-042-201) as per manufacturer's instructions. Viable cells were counted and plated in 24-well plates at 2.5–10 × 10^5 cells/well in 500 μl TIL media, which help preserve viability of both melanoma and immune cell cultures.[11] Adhered melanoma cells and suspension immune cells were treated with 10 nM dabrafenib and 1 nM trametinib or DMSO control and incubated for 48 h. Drug concentration was selected based on previously optimized cell culture conditions.[12] Adherent and suspension cell cultures were trypsinised and collected after treatment, washed in PBS and incubated on ice for 30 min with fluorescently labelled monoclonal antibodies (Supplementary Table S1) and Fc block (BD Biosciences, Australia). For intracellular staining, cells were fixed and permeabilized using the Transcription buffer Fixation/Permeabilization kit (ThermoFisher Scientific), stained with antibodies against the intracellular proteins (Supplementary Table S1), then washed. Samples were acquired on a 5 laser BD LSR Fortessa X-20 flow cytometer (BD Biosciences) as previously described.[13] Gating strategy for major cell populations are shown in Supplementary Figure S13.

The MEK1/2 inhibitor trametinib (GSK1120212) and BRAF inhibitor dabrafenib (GSK2118436) were purchased from Selleck Chemicals (Houston, TX, USA) and prepared as 1 mM stocks in DMSO.

Single-cell transcriptome sequencing

Single-cell tumour dissociates were thawed into TIL media, washed, counted and plated (up to 1 × 10^6 cells/well in 500 μl TIL media) in 24-well plate prior to treatment with 10 nM dabrafenib and 1 nM trametinib or DMSO control for 48 h. Adherent (melanoma) and suspension (immune cells) cell cultures were trypsinised and collected after treatment, washed in PBS, and enriched for viable cells using the Dead Cell Removal kit (Miltenyi Biotec, Cat no: 130-090-101) and MS columns (Miltenyi Biotec, Cat no: 130-042-201) as per manufacturer's instructions. Viable cells were resuspended in 0.04% BSA in PBS, filtered through a 30 μm filter and resuspended to a final concentration of 1000 cells/μl. Single-cell RNA sequencing libraries were generated using the 10× Genomics Chromium Single Cell 3′ Kit vs 3.1 and the 10× Chromium Controller according to manufacturer's protocol (10× Genomics, Pleasanton, CA, USA). Briefly, approximately 10,000 single cells were loaded to the Chromium Controller with a targeted recovery of at least 5000 cells. The cells were partitioned into Gel Beals in Emulsion Sequencing and quality control of the libraries was performed on a NovaSeq S4 by the Australian Genome Research Facility (AGRF, Australia). On average, 200 Gb of raw data were generated for each sample.

Melanoma cell culture

Tumour dissociates were plated into 24-well plates (1 × 10^6 cells/well) to isolate short-term patient-derived melanoma cell lines. Melanoma cell lines were maintained in complete DMEM (Dulbecco's Modified Eagle medium) supplemented with 10% heat-inactivated fetal bovine serum (Sigma), 4 mM glutamine (Sigma), and 20 mM HEPES (Sigma) at 37 °C in 5% CO_2. Cell authentication and profiling of cell lines were confirmed using the StemElite ID system from Promega. All cells tested negative for mycoplasma (MycoAlert Mycoplasma Detection Kit, Lonza, Basel). RNA sequencing data of the cell lines has been previously generated[13] and deposited in the Sequence Read Archive under the accession code PRJNA818797.

MTT metabolic assay

Melanoma cells were pre-treated with TNFα (1000 U/ml, PeproTech, Rocky Hill, NJ, USA Cat no: 300-01), IL-6 (25 ng/ml, PeproTech, Cat no: 200-06) or 0.1% BSA control for 72 h, then seeded in 96-well plates (1.5–2.0 × 10^3 cells/well) in complete DMEM. Media was removed the following day and melanoma cells exposed to increasing concentrations of the BRAF inhibitor dabrafenib (0, 1, 2.5, 5, 10, 50, 100, 500, 1000 and 5000 nM) and the MEK inhibitor trametinib (0, 0.1, 0.25, 0.5, 1, 5, 10, 50, 100 and 500 nM) at a 10:1 ratio for 72 h in the presence or absence of TNFα (1000 U/ml) or IL-6 (25 ng/ml). Cell viability was measured using the Luminescent CellTiter-Glo® 2.0 Assay reagent (Promega, Madison, WI, USA). Luminescence readings were acquired on a PHERASTAR FS microplate reader (BMG LABTECH, Germany). Cell viability was calculated as a percentage normalized to controls after background subtraction. A minimum of three independent viability assays were performed for each cell line in triplicate. The IC_{50} (half maximal inhibitory concentration) was generated from dose–response curves fitted using a comparison of three-parameter regression fit or four-parameter regression fit in GraphPad PRISM software (GraphPad). Area under curve (AUC) analysis was performed in GraphPad and the AUC values were used for statistical comparison (unpaired t-test, compared to control treatment).

Western blotting

Melanoma cells were pre-treated with TNFα (1000 U/ml, PeproTech, Rocky Hill, NJ, USA Cat no: 300-01), IL-6 (25 ng/ml, PeproTech, Cat no: 200-06) or 0.1% BSA control for 72 h, then collected for western blot analysis. Total cellular proteins were extracted, resolved on 10% SDS-polyacrylamide gels and transferred to PVDF-FL membranes (Millipore) for 2 h. Western blots were blocked for 1 h with 5% skim milk in Tris buffered saline (TBS) and probed with antibodies against total STAT (1:1000, Cell Signaling Technology; Cat no: 9139, AB_331757), phosphorylated STAT (1:1000, Cell Signaling Technology; Cat no: 9145, AB_2491009), IκBα (1:1000, Cell Signaling Technology; Cat no: 4814, AB_390781) and β-actin (1:6000, Sigma, Cat no: A5316, AB_476743). Secondaries used were goat anti-mouse immunoglobulin HRP and goat anti-rabbit immunoglobulin HRF (1:6000, Agilent Dako, Santa Clara, CA) and blots were imaged using ChemiDoc MP.

Analysis of hallmark signatures in melanoma cell cultures

Transcriptome data of previously RNA-sequenced melanoma cell lines were retrieved from the Sequence Read Archive under accession code PRJNA818797. FPKM values were used for ssGSEA[14] to derive the absolute enrichment scores using the gene sets from the Molecular Signature Database version 6.2[15] and to determine the melanoma differentiation transcriptome subtypes (undifferentiated, neural crest-like, transitory and melanocytic) using the support vector machine "top-scoring pairs" scripts kindly provided by Dr T. Graeber.[6] These transcriptome subtypes correspond to the differentiated (melanocytic and transitory) and de-differentiated melanoma phenotypes (neural crest-like and undifferentiated).[6,16]

scRNA-seq data processing and quality control

scRNA-seq counts were generated using the CellRanger 10× pipeline (v 3.1.0) to map the reads on to the human reference genome (GRCh38). We first performed quality control to include cells with number of total UMI less than 80,000 and greater than 500, number of genes greater than 400 and mitochondria genes expressed less than 20%, resulting in 168,599 cells for the downstream analysis. We then used Bioconductor R package *scater* to perform the data processing step.[17] The counts matrix was first size-factor standardized and log-normalized using *logNormCount* function. Next, we selected the top 2000 highly variable genes (HVGs) using function across patients. UMAP embedding was then generated on the top 20 PCs generated using the top HVGs for visualization.

Cell type annotation

We used scClassify[18] to annotate the broad cell types using two published melanoma datasets as reference[19,20] with a two-step procedures: In the first step, the cells are annotated by scClassify trained from the two reference separately; In the second step, the cells with the consistent annotations across two datasets are used to train a new scClassify model and annotate the cells with inconsistent annotations from the first step. We performed Numbat (v1.1.0)[21] to infer allele-specific CNV in single cells using 1000G hg38 Genome reference and SNP VCF. The reference expression profile is generated based on scClassify annotation.

Malignant cell state annotation

We focused on the cells that are classified as malignant cells in both scClassify and Numbat. The initial analysis reveals that apart from melanoma cell states, there are other cell states, including cell cycle, inflammatory and drug treatment effect in the full datasets which hinder clustering methods to identify melanoma subcellular states. There is also a lack of existing single-cell reference datasets of melanoma cell states. Therefore, we developed an approach to annotate the malignant cell state using a combination of unsupervised and supervised learning techniques. Firstly, we selected the cells from the DMSO control samples without high cell cycle score and inflammatory score as a reference dataset. The cell cycle score is based on the cell cycling signature provided by Seurat[22] and the inflammatory score is based on the Hallmark_Inflammatory_Response gene set.[15] This approach ensures that the analysis is not biased by cell cycle and inflammatory signals and minimally alters the original gene expression matrix. The threshold of high cell cycling score is determined by fitting a normal mixture model on both scores of G2M phase and S phase respectively and the threshold of inflammatory score is set as 0.4. To annotate the cell states of the DMSO control reference dataset, we first performed scMerge2[23] to remove the patient effect using the unsupervised setting, with number of unwanted variation to be removed set as 20, number of neighbour set as 10 and highly variable genes set as the melanoma cell states markers. Next, we performed principal component analysis on the integrated data and visualized the data by performing UMAP on the first 10 principal components. Then we built a shared nearest neighbour graph with K equal to 30 using *buildSNNGraph* function in *scran* package and performed clustering using Louvain clustering with *cluster_louvain* function in *igraph* package, resulting in four clusters in total.[24] We then annotated the four clusters as melanocytic, transitory, neural crest-like and undifferentiated, based on the cell type markers reported in.[6] Finally, we trained a scClassify model using the annotated DMSO control reference dataset to predict and obtain annotations for the remaining malignant cells in the dataset.

Quantification of the MAPK activity and responder classification

We used the common genes in two published MAPK signalling gene sets[25,26] to quantify the MAPK activity score for each cell. The cell-level MAPK activity scores are calculated from the trimmed mean expression of the genes from the selected gene set, with the 10% low expressed genes trimmed. We consider the cells in the DT samples with MAPK activity scores greater than 20% quantile of the patient-matched DMSO-treated cell state as nonresponder cells and less than 5% quantile as responder cells to generate equivalent numbers in both responder vs nonresponder groups for subsequent comparison. This comparison was further validated by varying the threshold for defining responder and nonresponder cells and by using a continuous variable. To determine whether the change of MAPK activity score is significantly different across cell type, we first calculated the cell-type specific difference of the average MAPK activity score for each patient. We then performed linear mixed model with ~cell_type + (1|patient) using function *lmer* from R package *lmerTest*.[27]

Differential expression analysis of responder and nonresponder cells

We aggregated cell type-specific expression profile of each patient across the responder and nonresponder cell groups by summing up the counts within each group. Therefore, for each cell type, we have a responder and a nonresponder gene by sample expression profile. We then performed edgeR with responder or nonresponder as covariates to identify the genes that are differentially expressed between responder and nonresponder cells. The genes are then ranked by logFC. The preranked based gene set enrichment analysis (GSEA) of the Hallmark gene sets[15] is performed using the fgsea function in the R package fgsea v1.22.0.[28]

Statistical analysis

Statistical analysis was performed in GraphPad Prism software v10 or using the R statistical software v4. Figure legends specify the statistical analyses used and define error bars.

Role of funders

The funders had no role in study design, data collection, interpretation, or writing of this work for publication.

Results

Treatment naive and immune checkpoint inhibitor-resistant melanoma tumours show heterogenous response to BRAF/MEK inhibitors

To explore the molecular features of BRAF/MEK inhibitor response in differentiated and dedifferentiated melanoma, we selected ten patients with metastatic $BRAF^{V600}$–mutant cutaneous melanoma; five patients were treatment naive (NAIVE) and five patients had progressed on first-line anti-PD-1 based therapy (IO PROG; anti-PD-1 monotherapy [nivolumab]: n = 1; anti-PD-1 and anti-CTLA-4 combination therapy [ipilimumab + nivolumab]: n = 4). Patient clinicopathologic features are shown in Table 1 and selection of patients and samples are detailed in Materials and Methods. The median patient age was 60 years (range 25–78) for the NAIVE group and 46 years (range 31–77) for the IO PROG group. The two treatment groups had the same proportions of males (80%), and all patients had a $BRAF^{V600E}$ mutation. Melanoma biopsies were derived from lymph node (7/10, 70%), bowel (2/10; 20%) and subcutaneous chest (1/10, 10%) and were processed into single-cell dissociates. Dissociates were treated *ex vivo* with DMSO vehicle control or combination BRAF/MEK inhibitors (DT; 10 nM dabrafenib and 1 nM trametinib). Forty-eight hours post treatment, the dissociates were analysed by flow cytometry and single-cell RNA sequencing (scRNA-seq) (Fig. 1a).

Initial flow cytometric profiling of the tumour dissociates revealed a range of melanoma and immune T cell content that did not reflect prior treatment. For instance, melanoma content ranged from 49 to 94% and 18–88% in the baseline NAIVE and IO PROG samples, respectively. Similarly, T cell content was variable, and ranged from 2 to 24% (CD4+ T cells) and 1–14% (CD8+

Characteristics	NAIVE (n = 5)	IO PROG (n = 5)
Age[a], median (range)	60 (25–78)	46 (31–77)
Sex, n (%)		
Male	4 (80)	4 (80)
Female	1 (20)	1 (20)
Prior treatment, n (%)		
None	5 (100)	
PD-1 inhibitor		1 (20)
PD-1+CTLA-4 inhibitor		4 (80)
Mutation, n (%)		
BRAF V600E	5 (100)	5 (100)
LDH, n (%)		
Normal	3 (60)	4 (80)
Elevated	2 (40)	1 (20)
Site, n (%)		
Lymph node	3 (60)	4 (80)
Bowel	1 (20)	1 (20)
Subcutaneous chest	1 (20)	
Stage at diagnosis, n (%)		
Stage I	3 (60)	
Stage II	2 (40)	1 (20)
Stage III		3 (60)
Stage IV		1 (20)

[a]Age at time of biopsy shown.

Table 1: **Baseline clinicopathologic features of patients with melanoma.**

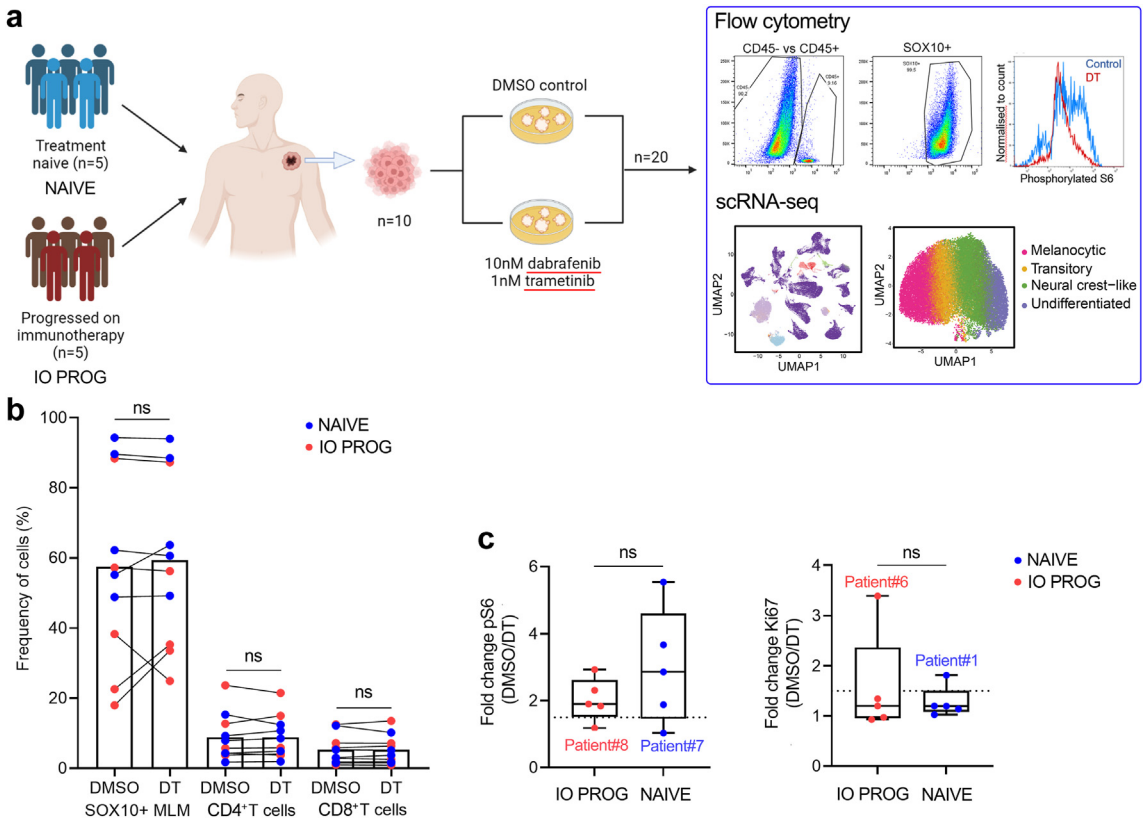

***Fig. 1:* Flow cytometric profiling of tumour dissociates.** a) Schematic of the study design. b) Percentage of melanoma (CD45−/SOX10+), CD4+ (CD45+/CD4+) and CD8+ (CD45+CD8+) T cells in tumour dissociates of patients with melanoma (n = 5, treatment naive, NAIVE, blue; n = 5, progressed on PD-1-based therapy, IO PROG, red) following treatment with DMSO control or combination BRAF/MEK inhibitors dabrafenib and trametinib (DT, 10 nM and 1 nM, respectively). Percentages shown as a proportion of live viable cells in the samples. Cell frequencies for each sample are shown in Supplementary Table S2 and gating strategy of cells shown in Supplementary Figure S13. c) Boxplots showing fold change in phosphorylated S6 and Ki67 levels (median fluorescence intensity (MFI) of DMSO control/MFI DT) in NAIVE (blue) and IO PROG (red) tumour dissociates. Dotted line indicates a 1.5-fold difference. Data comparison between DMSO and DT performed using paired t-test while comparison between IO PROG and NAIVE performed using unpaired t-test; ns, not significant.

T cells) in all tumour dissociates. As expected, short-term treatment with DT did not significantly or consistently change tumour (SOX10+ melanoma cells) or T cell (CD4+ and CD8+) proportions in the NAIVE or the IO PROG samples (Fig. 1b, Supplementary Table S2). Approximately 80% of tumour samples showed a decrease in phosphorylated S6 in melanoma cell populations after DT treatment (median reduction 2.1-fold, range 1.0–5.5-fold), indicative of MAPK signalling inhibition (Fig. 1c). Only the NAIVE sample from Patient 7 and IO PROG sample from Patient 8 showed minimal change in phosphorylated S6 with DT treatment. Two samples (IO PROG from Patient 6, and NAIVE from Patient 1) showed a notable decrease (3.4-fold and 1.8-fold, respectively in Ki67 expression; median 1.2-fold, range 0.9–3.4-fold), suggesting minimal downstream proliferative arrest in the majority of samples within the 48 h treatment time frame (Fig. 1c). These data confirm that DT-induced signalling changes can be examined *ex vivo* in melanoma single-cell dissociates.

Single-cell transcriptome analysis identifies dedifferentiated melanoma states enriched in immunotherapy progressing tumours

Single-cell transcriptome sequencing (scRNA-seq) was performed on the tumour dissociates after treatment with DMSO control or DT. In order to interrogate melanoma cell state-specific responses to DT, we developed a framework that combined supervised and unsupervised learning to leverage information from two public scRNA-seq datasets[19,20] and melanoma cell state signatures[6] (Fig. 2a). In the first component of our framework, the broad cell types present in each tumour biopsy were annotated using scClassify[18] with two previously-published scRNA-seq datasets[19,20] as reference. After quality control (Supplementary Figure S1), this process identified nine main cell types, including B

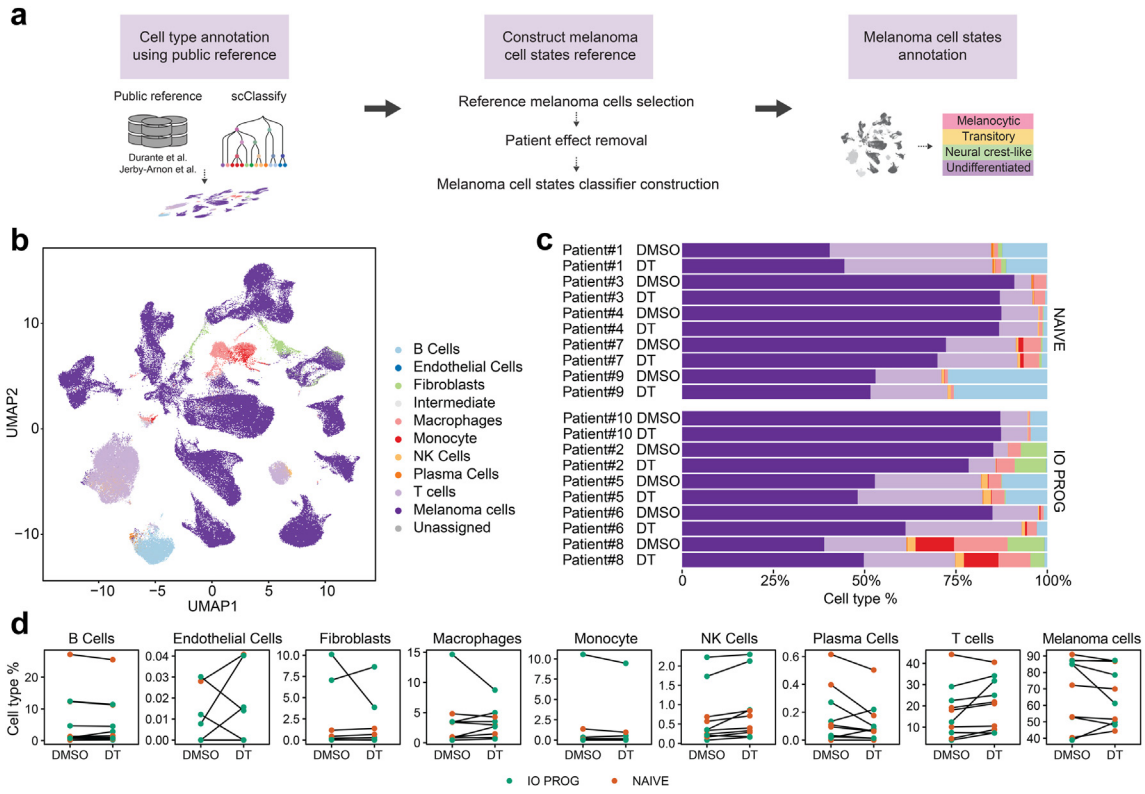

***Fig. 2*: Composition of malignant and non-malignant cell types in tumour dissociates.** a) Schematic showing the analytical framework applied to the scRNA-seq data combining supervised and unsupervised learning. b) UMAP (Uniform Manifold and Projection) plot of stromal, immune and melanoma cell types in the tumour dissociates. The nine clusters were annotated into cell types using differentially expressed gene sets and inferred copy number variations. c) Proportion of cell types in individual tumour samples treated with DMSO control or DT. d) Changes in cell type proportions in matched DMSO control or DT-treated tumour dissociates. Orange symbols indicate NAIVE while green symbols indicate IO PROG patient samples. Data comparison between DMSO vs DT, and NAIVE vs IO PROG performed using the linear mixed effect model; p values shown in Supplementary Table S3.

cells, endothelial cells (ECs), fibroblasts, macrophages, monocytes, natural killer (NK) cells, plasma cells, T cells and melanoma cells (Fig. 2b); cell type annotations were supported by the expression of known cell type markers (Supplementary Figure S2). Annotation of melanoma cells was further confirmed by applying Numbat,[21] a computational algorithm that inferred large-scale copy number variations (CNV) in the tumour cell clusters (Supplementary Figure S3), where 98.1% of cells annotated as tumour by scClassify were confirmed by Numbat. Fig. 2b gives a visual representation of the data, where melanoma cells formed separate clusters according to patient tumour while non-malignant cells clustered primarily by cell type (Fig. 2b, Supplementary Figure S4). Proportions of melanoma and T cells annotated using scClassify correlated well with the CD45−/SOX10+ melanoma (r = 0.70, Pearson correlation) and CD45+ CD4+ and CD8+ T cells (r = 0.73, Pearson correlation) identified by flow cytometric profiling (Supplementary Figure S5). In each tumour sample, we detected melanoma, stromal and immune cell types (Fig. 2c) with melanoma cells representing the predominant cell type (range 39–91%, median 71% of total cells). Cell type proportions, with the exception of NK cells, did not significantly change in response to DT treatment and were not significantly different between NAIVE and IO PROG groups (Fig. 2d, Supplementary Table S3). Only one tumour sample (IO PROG, Patient 6) showed a considerable decrease in melanoma cell numbers with DT treatment, and this aligned with the ~3-fold reduction in Ki67 expression and ~1.8-fold reduction in S6 phosphorylation (Fig. 1C) in this sample.

We next focused on characterizing and enumerating the distinct melanoma cell states. Due to the lack of a single-cell melanoma differentiation state cohort, we generated a reference subset from the DMSO control-treated tumour dissociates after adjusting for patient effect using scMerge[29] (Fig. 3a, Supplementary Figure S6). This was done by first separating the cell states using unsupervised clustering followed by annotating each cluster using previously defined, trajectory-

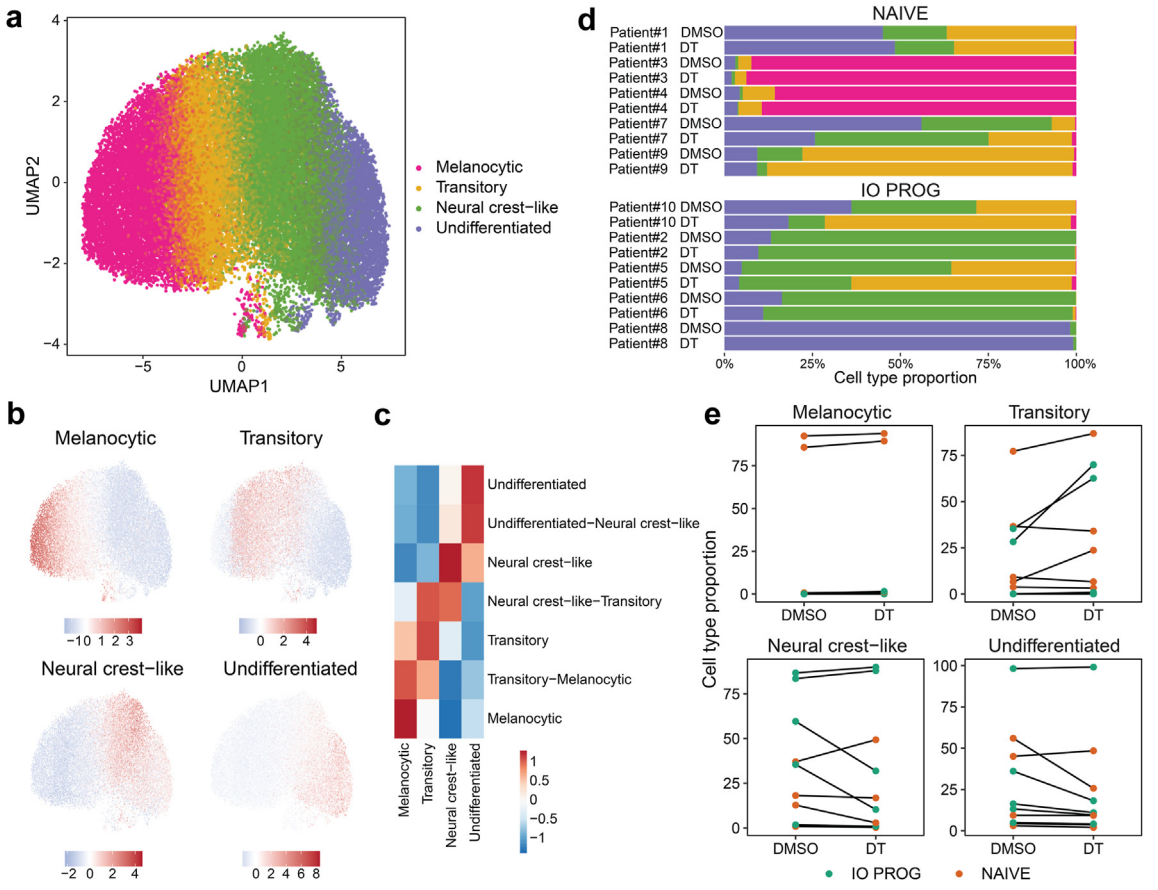

***Fig. 3*: Distinct melanoma cell states identified in tumour biopsies.** a) UMAP plot of aggregated (from all 20 samples) malignant melanoma cells showing four cell clusters, annotated as melanocytic, transitory, neural crest-like and undifferentiated. b) UMAP plot and c) heatmap showing the relative expression of the progressive differentiation gene signatures[6] in the four cell clusters. Scale bars shows relative high (red) vs low (blue) expression of the signatures. d) Proportion of melanoma cell states in individual tumour samples treated with DMSO control or DT. e) Changes in cell state proportions in matched DMSO control or DT-treated tumour dissociates. Orange symbols indicate NAIVE while green symbols indicate IO PROG patient samples. Data comparison between DMSO and DT, and NAIVE vs IO PROG performed using the linear mixed effect model; p values shown in Supplementary Table S4.

informed transcriptomic signatures of melanoma differentiation states.[6] This resulted in identification of four discrete melanoma cell states; melanocytic, transitory, neural crest-like and undifferentiated (Fig. 3b and c, Supplementary Figure S7). We validated this approach using published melanoma scRNA-seq datasets[20,30] and identified the same four cell states in these datasets (Supplementary Figure S7). Importantly, we also confirm the quality of our scRNA-seq data which was derived from 3000 to 12,500 melanoma cells per tumour sample, far exceeding tumour cell numbers sequenced (~50–2000) in previous studies.[20,30] This enabled the detailed analyses of individual melanoma cell states and treatment effects at the single-cell level.

Next, we built a melanoma cell state model using the annotated tumour cell states from DMSO control as reference, and annotated the remaining tumour cells in the DT-treated samples (see methods for additional details). Examination of the expression of key differentiation markers (e.g., AXL, MITF, SOX10 and NGFR) further confirmed differences in cell states in the four clusters (Supplementary Figure S8).

The proportions of each melanoma cell state remain largely unaffected by DT treatment (Fig. 3d and e, Supplementary Table S4). However, we noted enrichment of both neural crest-like and undifferentiated melanoma cells in IO PROG compared to NAIVE samples. For instance, the median proportion of neural crest-like cells at baseline in the IO PROG group was 60% compared to 12.8% in the NAIVE group, and similarly, the median proportion of undifferentiated cells was 16.3% vs 9.3% in IO PROG and NAIVE, respectively (Supplementary Figure S9). The proportion of dedifferentiated cells (neural crest-like and undifferentiated combined) was significantly higher in the IO PROG group compared to the NAIVE group (unpaired

t-test, p = 0.0324, Supplementary Figure S9A). Interestingly, the proportions of transitory cells in each tumour sample at baseline positively correlated with the degree of phosphorylated S6 reduction (r = 0.6344, p = 0.049, Pearson correlation), while the proportion of neural crest-like and undifferentiated cells was negatively correlated with the degree of phosphorylated S6 reduction (r = –0.2385 and r = –0.2001, respectively, Pearson correlation), although this was not significant (Supplementary Figure S9B). It is important to note that not all patient samples contained cells representing all four differentiation states, and in fact, it was rare to find all four cell states co-existing in a tumour sample. For example, tumour from Patient 8 consisted of predominantly undifferentiated cells (98% of total melanoma cells at baseline) whereas Patient 3 and Patient 4 tumours contained predominantly melanocytic cells (92% and 86% of total melanoma cells at baseline, respectively; Fig. 3d). Because melanocytic cells were largely present in only two patient samples, and given that melanocytic and transitory melanoma cells have similar differentiation marker profiles[6], we grouped these two states and henceforth refer to this group as differentiated cells.

Discriminating melanoma cell state-specific responses using a computational framework

To examine tumour-associated signalling changes resulting from *ex vivo* DT treatment, we first compared gene expression profiles of DMSO control vs DT-treated tumour cells. Critically, gene set enrichment analysis confirmed the DT-induced downregulation of Hallmark proliferative gene sets (E2F_Targets, G2M_Checkpoint, MYC_targets_V1, MYC_targets_V2) and MAPK signalling gene sets[25,26] in all cell states (Supplementary Figure S10).

We extended the analyses to examine tumour cell responses to DT within each cell state. A computational framework was developed to infer the treatment-specific effects in tumour cells using two published MAPK signalling gene sets[25,26] as a surrogate score for MAPK pathway activity. The differentiated, neural crest-like and undifferentiated tumour cell states showed comparable baseline MAPK activity (Fig. 4a). However, MAPK activity was significantly downregulated in differentiated (linear mixed effect model, p = 0.023) and neural crest-like cells (linear mixed effect model, p = 0.017) compared to undifferentiated cells in response to DT treatment (Fig. 4a). MAPK activity suppression was variable between patient tumours and overall, undifferentiated cells appear least responsive compared to other cell states within the same tumour (Supplementary Figure S11). However, undifferentiated cells also show variable responses to DT. For instance, Patient 8 tumour consisted of 98% undifferentiated cells and these cells showed minimal downregulation (~0.9-fold) of MAPK activity score in response to DT treatment (Supplementary Figure S11). The scRNA-seq data are concordant with the flow cytometry analysis of this sample, showing limited suppression of phosphorylated S6 (Fig. 1c). In contrast, Patient 6 tumour consisted of 84% neural crest and 16% undifferentiated cells, and both cell states were responsive to DT, showing a 2.7 and 2.0-fold reduction in MAPK activity score post DT treatment, respectively (Supplementary Figure S11). It is worth noting that this tumour also showed the greatest reduction in cell proliferation (~3.4-fold) and considerable decrease in phosphorylated S6 (~1.8-fold) in response to DT treatment (Fig. 1d).

Our data suggests that the undifferentiated melanoma state is not inherently resistant to DT. Indeed, in most tumour samples, treatment with DT decreased MAPK activity in undifferentiated melanoma cells. In order to define the signalling networks associated with DT response and resistance, melanoma cells were stratified into two categories: responding or non-responding. Responding and nonresponding tumour cell states were defined as having a MAPK activity score, post DT treatment, within the lowest 5% or highest 20% MAPK activity score of the patient-matched DMSO-treated cell state, respectively. This approach identified responding and nonresponding tumour cells in all cell states (Fig. 4b), although there were more non-responding undifferentiated cells (nonresponding cells comprise 75% undifferentiated, 9.7% neural crest-like and 14.8% differentiated cells in DT-treated tumours). Importantly, approximately 7% of undifferentiated tumour cells (~6% of all responding cells in DT-treated tumours) responded to DT, and these responsive cells showed a DT-induced decrease in MAPK activity score equivalent to responding differentiated tumour cells.

Gene set enrichment analysis (GSEA) of the Hallmark signatures was performed on the responding and nonresponding cells within each cell state in the DT-treated samples, and a normalized enrichment score (NES) was derived based on the size of the gene sets and the enrichment score (Fig. 4c). All nonresponding cells regardless of cell state showed enrichment in the Hallmark inflammatory response, IL6, IL2 and TNFA signalling, hypoxia and epithelial to mesenchymal gene sets, suggesting that these nonresponding cells may induce inflammatory transcriptional programs that contribute to their resistance to treatment. In contrast, only differentiated responding cells showed consistent enrichment of Hallmark proliferative gene sets (e.g., oxidative phosphorylation, E2F targets), suggesting that highly proliferative differentiated melanoma cells may be more responsive to DT treatment.

Tumour-intrinsic pro-inflammatory IL6 and TNFα signalling contributes to BRAF/MEK inhibitor resistance

Given that IL-6 and TNFα signalling pathways were significantly elevated in nonresponding cells and

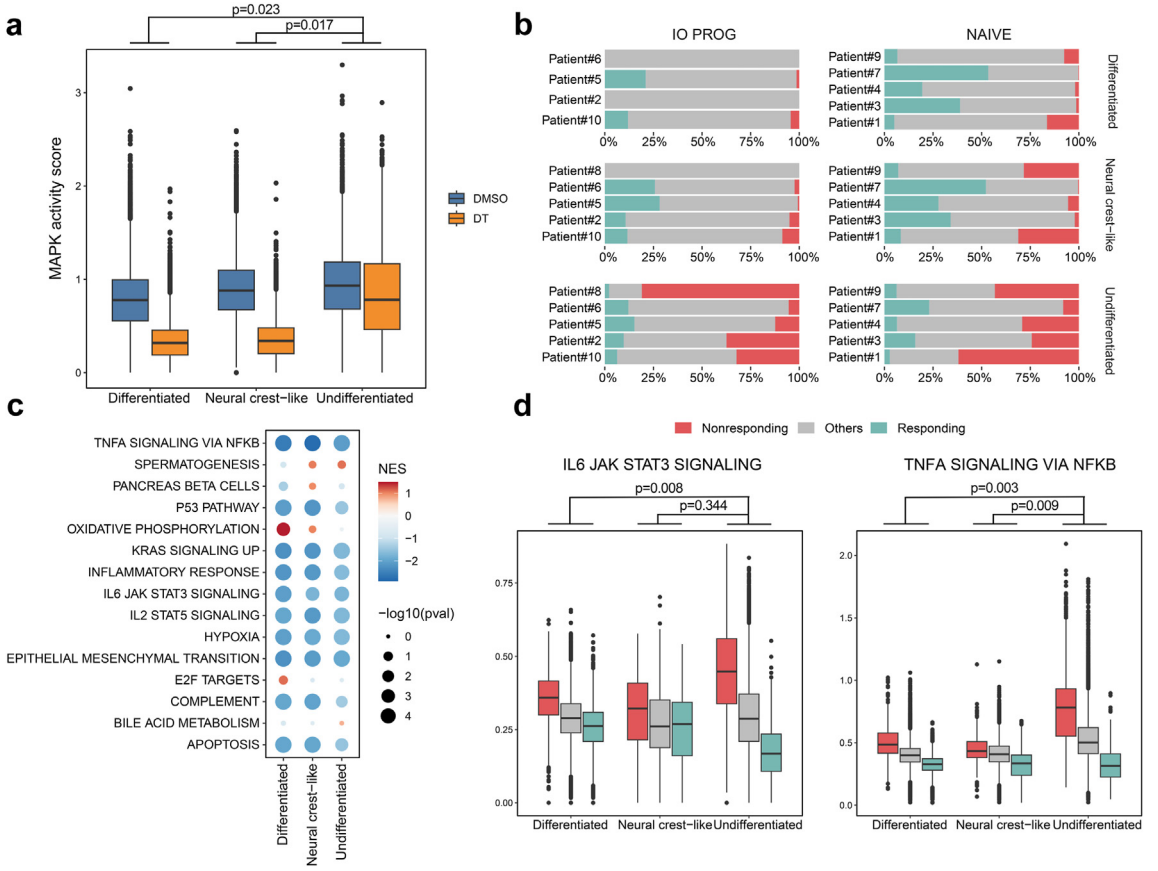

***Fig. 4*: Cell-state specific responses to DT treatment.** a) MAPK activity score (assessed using the expression of common genes in two MAPK pathway gene sets[25,26]) in DMSO control (blue) and DT-treated (orange) differentiated, neural crest-like and undifferentiated cells. Data comparison performed using the linear mixed effect model. b) Proportion of responding (teal) and nonresponding (red) cells in each patient's DT-treated tumour samples, arranged by cell state. c) Gene set enrichment analysis of the Hallmark signatures in responding and non-responding melanoma cells in DT-treated samples, analysed using edgeR. Comparison separated by cell state and normalized enrichment score (NES) and p values shown. d) Expression of the Hallmark IL6 and TNFA signalling gene sets in responding (teal) and nonresponding (red) melanoma cells categorized by cell state. Data comparison performed using the linear mixed effect model.

enriched in the undifferentiated cell state (Fig. 4d), we investigated whether activation of these pathways contribute to DT resistance. A panel of short-term melanoma cell lines (n = 13) with matched transcriptome data were assessed for their sensitivity to DT using MTT metabolic assays. Trametinib IC_{50} values were derived from the MTT assays and correlated with the Hallmark gene sets, with the Hallmark Apoptosis, TNFA and IL6 signalling gene sets showing significant and strong positive correlation ($r > 0.85$, $p < 0.001$, Pearson correlation, Fig. 5a) with trametinib IC_{50} values. In particular, melanoma cell lines with elevated ssGSEA scores for the Hallmark TNFA and IL-6 signalling gene sets also showed high trametinib IC_{50} values, and the IC_{50} values were significantly correlated with the ssGSEA scores ($r = 0.8692$, $p = 0.0001$ and $r = 0.8619$, $p = 0.0002$, respectively, Pearson correlation, Fig. 5b). It is also worth noting that undifferentiated cell lines, which were classified based on their transcriptome profiles,[6] also showed higher Hallmark TNFA and IL-6 signalling gene set expression (Fig. 5b). Similarly, we found positive correlation between the trametinib IC_{50} values and ssGSEA scores for the Hallmark TNFA and IL-6 signalling gene sets in the Cancer Cell Line Encyclopedia (CCLE) dataset ($r = 0.24$ and $r = 0.21$, respectively, Pearson correlation, Supplementary Figure S12). Overall, these data indicate that sensitivity to DT is associated with TNFα and IL-6 pathway activity and these pathways are enriched in nonresponding undifferentiated cells.

To further validate that activation of tumour-intrinsic IL6 and TNFα signalling pathways influence melanoma response to DT, melanoma cells were pre-treated with TNFα (1000 U/ml) or IL-6 (25 ng/ml) for 72 h, then treated for a further 72 h with increasing concentration of combination DT in the presence or absence of IL6 or

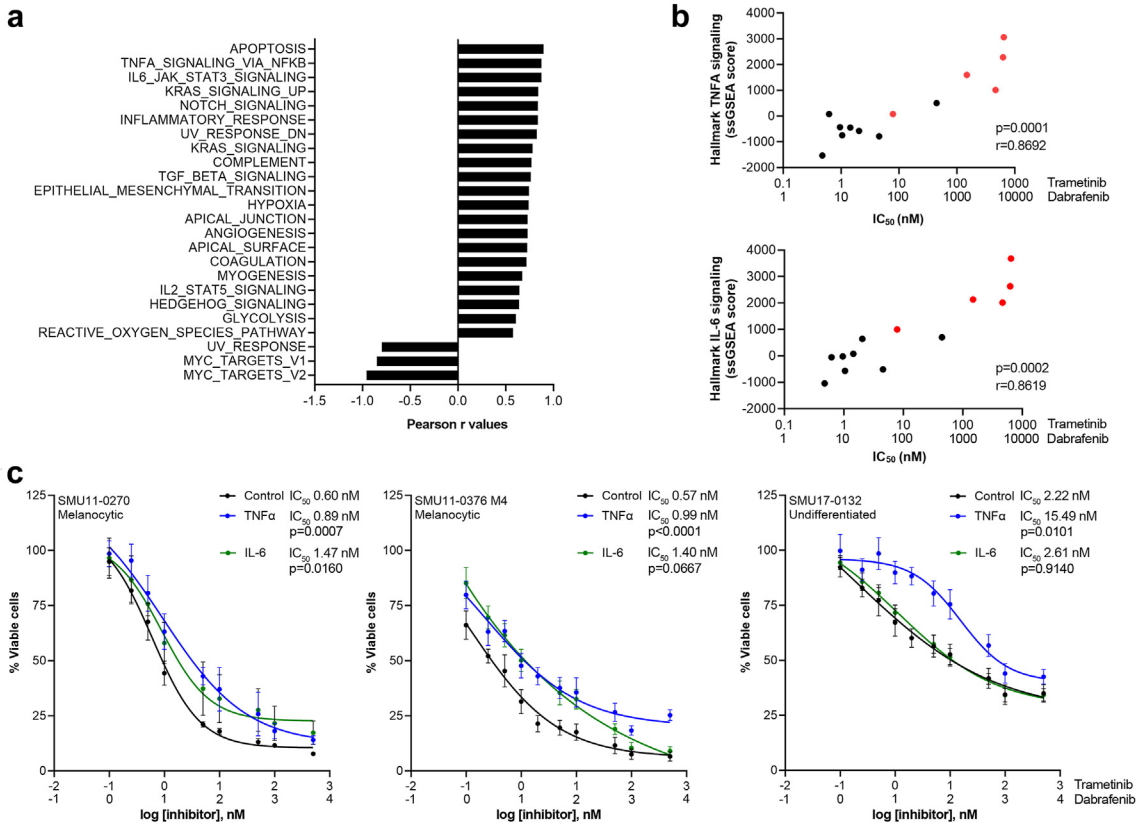

Fig. 5: **TNFα and IL-6 signalling influence response to BRAF/MEK inhibitors.** a) Correlation between the MAPK inhibitors dabrafenib and trametinib IC_{50} values and Hallmark gene sets. Data analysed using Pearson correlation, correlation with $p < 0.01$ shown and Pearson r coefficient values plotted on the x axis. b) Scatterplots showing correlation of the Hallmark TNFA and IL-6 signalling gene sets with dabrafenib and trametinib IC_{50} values in melanoma cell lines (n = 13). Undifferentiated melanoma cell lines highlighted in red. Pearson correlation is shown. c) Cell viability plots showing change in dabrafenib and trametinib IC_{50} values. Cells were pre-treated with IL6 (25 ng/ml) or TNFα (1000 U/ml) for 72 h, followed by treatment with increasing concentrations of dabrafenib + trametinib (DT, at 10:1 ratio) ± IL6 (25 ng/ml, green) or TNFα (1000 U/ml, blue) in the SMU11-0270 and SMU11-0376 M4 melanocytic and SMU17-0132 undifferentiated cell lines compared to control (0.1% BSA, black). Area under curve (AUC) analysis was performed and the AUC values were used for statistical comparison (unpaired t-test, IL6 or TNFα compared to control treatment, dabrafenib and trametinib IC_{50} values and p values shown). At least three biological replicates were performed for each cell line.

TNFα. Treatment with IL6 increased pSTAT (Tyr705) accumulation in the melanocytic SCC11-0270 and SMU11-0376 M4 cell lines, but not in the undifferentiated SMU17-0132 cell line, while treatment with TNFα decreased IkBα expression in all cell lines and this was more apparent in the SMU17-0132 cell line (Supplementary Figure S12).

Exposure to TNFα or IL6 induced marginally higher trametinib IC_{50} values in the melanocytic SMU11-0270 (1.5-fold difference for TNFα, $p = 0.0007$ and 2.5-fold difference for IL-6, $p = 0.0160$ compared to control, unpaired t-test) and SMU11-0376 M4 (1.7-fold difference for TNFα, $p < 0.0001$ and 2.5-fold difference for IL-6, $p = 0.0667$ compared to control, unpaired t-test) cell lines. In the undifferentiated SMU17-0132 cell line, exposure to TNFα alone, but not IL6, induced a 7-fold increase in IC_{50} value compared to control ($p = 0.0101$, unpaired t-test Fig. 5c). These results suggest that tumour-intrinsic pro-inflammatory IL6 and TNFα signalling influence response to DT, but the impact of treatment response may be tumour and cell line-specific, and dependent on the intrinsic and inducible levels of the pro-inflammatory signals.

Discussion

Immune checkpoint and BRAF/MEK inhibitors have significantly improved the survival of patients with advanced and high-risk early melanoma although treatment resistance remains a common challenge.[2,3,5] Studies uncovering treatment resistance mechanisms have relied on bulk genomic and transcriptomic data from tumour biopsies[11,31–34] but these analyses do not adequately account for heterogeneity within a tumour

biopsy. This has been mitigated in recent years with the introduction of single-cell sequencing technologies that enable assessment of genomic and molecular changes within individual cells.

In this study, we utilized tumour dissociates derived from patients who have progressed on immunotherapy and treatment-naive patients, to examine the molecular features of response to BRAF/MEK inhibitors in distinct melanoma differentiation states. Short-term *ex vivo* treatment of the tumour dissociates with DT effectively recapitulated early treatment-induced effects seen in patients,[12] with potent downregulation of ribosomal protein S6 signalling in melanoma cells indicative of MAPK activity suppression.[35,36]

To uncover mechanisms underlying response to DT, tumour dissociates were scRNA-seq following *ex vivo* DT treatment. Although the sample size (n = 20) was limited, the comprehensive single-cell data generated, from patient-matched *ex vivo*-treated specimens, and the abundance of tumour cells (3000–12,500 melanoma cells per sample; Supplementary Figure S7B) afforded a unique opportunity to rigorously analyse the treatment-induced effects and influence of melanoma cell states at the individual cell level. To effectively compare the data, we first developed and implemented an integrated computational biology workflow 1) employing scClassify[16] combined with supervised annotation for more iterative and precise identification of cell subsets and 2) merging the melanoma cell transcriptome data using scMerge[18] for informed cell state annotation using previously defined transcriptome signatures.

Implementation of this integrated methodology enabled identification of four discrete melanoma cell states, and here, we report that dedifferentiated melanoma cells with neural crest-like or undifferentiated transcriptomic signatures are enriched in tumour dissociates from patients who have progressed on immunotherapy. Moreover, we show that each tumour differed in the composition and proportion of these melanoma states. For instance, of the 10 tumour biopsies included in this study, only one biopsy (Patient 8) consisted of a predominant undifferentiated cell state while the majority contained a mixture of two or three cell states. Hence, heterogeneity in treatment response is likely due to the presence of these preexisting cell states, each with differing signalling activity and treatment responses.

Dedifferentiated melanoma cells have been reported to be resistant to both immune-based and BRAF/MEK inhibitor therapies.[7–9] Dedifferentiated cells are enriched after treatment with BRAF/MEK inhibitors[10,37] and we also identified abundant dedifferentiated cells in biopsies of patients who have progressed on immunotherapy compared to treatment-naive patients. The transition to dedifferentiated melanoma is stimulated by the pro-inflammatory tumour microenvironment, with elevated TNFα, TGFβ and IFNγ known to induce melanoma dedifferentiation *in vitro*.[11,38,39] Thus, treatment with immunotherapy would heighten the pro-inflammatory milieu, inducing melanoma dedifferentiation and the subsequent selection of immunotherapy and molecular therapy resistance. This model of resistance is supported by data from the SECOMBIT clinical trial[40]; patients with melanoma showed diminished response to BRAF/MEK inhibitors after progression on combination immune checkpoint inhibitors compared to first-line BRAF/MEK inhibitor therapy (overall response rate of 87% in first line vs 58% in second line). Furthermore, BRAF/MEK inhibitor response after progression on PD-1 inhibitor in the KEYNOTE-006 cohort was only 30.5%.[41] These clinical trials highlight that the selection and sequencing of these treatment modalities are critical for optimal treatment response. For example, the DREAMseq trial reported that combination CTLA-4/PD-1 inhibitors followed by BRAF/MEK inhibitors is the preferred treatment sequence for patients with metastatic $BRAF^{V600}$-mutant melanoma. The 2-year overall survival for patients receiving first-line ipilimumab/nivolumab was 71.8% (95% CI, 62.5–79.1%) compared to 51.5% (95% CI, 41.7–60.4%) for patients treated initially with combination dabrafenib/trametinib.[42]

Several treatment resistance mechanisms have been proposed for dedifferentiated melanoma but these have been mostly associative and based on bulk tumour data. In this report, we developed an informed method to monitor treatment perturbations, by combining our computational biology workflow with known signatures of MAPK pathway activity,[25,26] to enable modelling of treatment response vs nonresponse based on the level of MAPK activity suppression. Using this approach, we identified subsets of responding and nonresponding cells in all cell states, and DT-responsive dedifferentiated cells were also identified. These data suggest that melanoma dedifferentiation does not preclude response to DT. In keeping with this, whilst dedifferentiated melanomas are attributed with treatment resistance, other studies have shown that the proliferative and pigmentation gene markers representative of the melanocytic differentiated state are associated with poorer response to immunotherapy[39] and poorer survival.[43] Overall, these findings indicate that dedifferentiation may not be sufficient to confer resistance as a proportion of dedifferentiated melanoma cells continue to respond to treatment.

Interestingly, comparison of responding and nonresponding cells revealed elevated expression of multiple pro-inflammatory pathways including IL6 and TNFα in the nonresponding cells, implicating these pathways in BRAF/MEK inhibitor resistance. Circulating IL6 and TNFα are elevated in patients with melanoma, particularly after treatment with BRAF/MEK and immune checkpoint inhibitors, and increased serum levels are associated with poor survival and increased treatment-

related adverse events.[44–46] We propose that dedifferentiated melanomas are less responsive to DT due to the higher pro-inflammatory activities. To address the limitation of small sample size, we further confirmed these findings in a large panel of melanoma cell lines (n = 13), showing dedifferentiated melanoma cells to be more resistant to DT treatment, and that these cell lines have elevated IL6 and TNFα pathway activity. We also show that activation of these pathways via exogenous IL6 and TNFα stimulation induced melanoma cells to be more resistant to DT, indicating that tumour-intrinsic IL6 and TNFα signalling contribute to MAPK inhibitor resistance. This finding aligns with a previous study reporting activation of NF-κB signalling by TNFα inducing MAPK inhibitor resistance.[47] Similarly, macrophage-derived TNFα has been shown to contribute to MAPK inhibitor resistance,[48] suggesting that a pro-inflammatory milieu propagates treatment resistance. Furthermore, our analyses show that multiple pro-inflammatory pathways are enriched in nonresponding cells, and the impact and precise role of these pathways in mediating treatment resistance warrant further investigation, as targeting one pathway may not be sufficient to overcome MAPK inhibitor resistance.

In conclusion, this study provides proof-of-concept that *ex vivo* treatment of tumour dissociates coupled with a unique single-cell computational biology approach enabled dissection of melanoma cell state-specific differences in treatment response. Our study provides a valuable framework to facilitate a more precise understanding of molecular mechanisms underlying heterogeneity in treatment response and assist in the identification of therapeutic targets and biomarkers for treatment resistance.

Contributors

SYL, YL and HR designed the study, analysed the data and wrote the manuscript. SYL, BP and AS conducted the experiments. YL and JYHY provided bioinformatic analysis and support. JHL, RAS and GVL provided clinical data and input. All authors read and approved the manuscript. SYL and YL have verified the underlying data reported in the manuscript.

Data sharing statement

The dataset generated and analysed in the current study are available from the corresponding author on reasonable request. Data is deposited to the Sequence Read Archive under the submission code PRJNA1145093. The code used in the single-cell RNA sequencing data analysis is provided as part of a git repository and can be accessed from https://github.com/SydneyBioX/MelanomaDT_2024 and from the following doi: https://zenodo.org/doi/10.5281/zenodo.12720636.

Declaration of interests

JHL has received honorarium from Merck, Sharp & Dohme and AstraZeneca, received conference support from Pfizer and Merck, Sharp & Dohme, and consulting fees from Boxer Capitol. JHL is a consultant for Merck, Sharp & Dohme, Sanofi, Cancer Council and EviO. RAS has received fees for professional services from MetaOptima Technology Inc., F. Hoffmann-La Roche Ltd, Evaxion, Provectus Biopharmaceuticals Australia, Qbiotics, Novartis, Merck Sharp & Dohme, NeraCare, AMGEN Inc., Bristol-Myers Squibb, Myriad Genetics, GlaxoSmithKline, IO Biotech ApS and SkylineDX B.V. GVL is consultant advisor for Agenus, Amgen, Array Biopharma, AstraZeneca, Bayer Health Care, BioNTech, Boehringer Ingelheim, Bristol Myers Squibb, Evaxion, Hexal AG (Sandoz Company), Highlight Therapeutics S.L., IO Biotech, Immunocore, Innovent Biologics USA, Merck Sharpe & Dohme, Novartis, PHMR Ltd, Pierre Fabre, Qbiotics, Regeneron, Scancell Limited and SkylineDX B.V. GVL has received conference support from Bristol Myers Squibb and Pierre Fabre. All other authors declare no conflicts of interest.

Acknowledgements

JHL is supported by a National Health and Medical Research Council of Australia (NHMRC) Investigator Grant. RAS is supported by a NHMRC Investigator Grant (2022/GNT2018514). Support from The Cameron Family Foundation as well as from colleagues at Melanoma Institute Australia and Royal Prince Alfred Hospital is also gratefully acknowledged. GVL is supported by a NHMRC Investigator Grant (2021/GNT2007839) and by the University of Sydney Medical Foundation, Australia. This work was supported by Macquarie University, Australia, Melanoma Institute Australia, Australia, and the National Health and Medical Research Council, Australia (NHMRC; grant 2012860, 2028055).

Appendix A. Supplementary data

Supplementary data related to this article can be found at https://doi.org/10.1016/j.ebiom.2024.105308.

References

1 Michielin O, Atkins MB, Koon HB, Dummer R, Ascierto PA. Evolving impact of long-term survival results on metastatic melanoma treatment. *J Immunother Cancer*. 2020;8(2):e000948.
2 Long GV, Swetter SM, Menzies AM, Gershenwald JE, Scolyer RA. Cutaneous melanoma. *Lancet*. 2023;402(10400):485–502.
3 Robert C, Grob JJ, Stroyakovskiy D, et al. Five-year outcomes with dabrafenib plus trametinib in metastatic melanoma. *N Engl J Med*. 2019;381(7):626–636.
4 Larkin J, Chiarion-Sileni V, Gonzalez R, et al. Five-year survival with combined nivolumab and ipilimumab in advanced melanoma. *N Engl J Med*. 2019;381(16):1535–1546.
5 Robert C, Ribas A, Schachter J, et al. Pembrolizumab versus ipilimumab in advanced melanoma (KEYNOTE-006): post-hoc 5-year results from an open-label, multicentre, randomised, controlled, phase 3 study. *Lancet Oncol*. 2019;20(9):1239–1251.
6 Tsoi J, Robert L, Paraiso K, et al. Multi-stage differentiation defines melanoma subtypes with differential vulnerability to drug-induced iron-dependent oxidative stress. *Cancer Cell*. 2018;33(5):890–904.e5.
7 Muller J, Krijgsman O, Tsoi J, et al. Low MITF/AXL ratio predicts early resistance to multiple targeted drugs in melanoma. *Nat Commun*. 2014;5(5712):5712.
8 Mehta A, Kim YJ, Robert L, et al. Immunotherapy resistance by inflammation-induced dedifferentiation. *Cancer Discov*. 2018;8(8):935–943.
9 Landsberg J, Kohlmeyer J, Renn M, et al. Melanomas resist T-cell therapy through inflammation-induced reversible dedifferentiation. *Nature*. 2012;490(7420):412–416.
10 Tirosh I, Izar B, Prakadan SM, Wadsworth MH 2nd, Treacy D, Trombetta JJ, et al. Dissecting the multicellular ecosystem of metastatic melanoma by single-cell RNA-seq. *Science*. 2016;352(6282):189–196.
11 Lee JH, Shklovskaya E, Lim SY, et al. Transcriptional downregulation of MHC class I and melanoma de- differentiation in resistance to PD-1 inhibition. *Nat Commun*. 2020;11(1):1897.
12 Long GV, Fung C, Menzies AM, et al. Increased MAPK reactivation in early resistance to dabrafenib/trametinib combination therapy of BRAF-mutant metastatic melanoma. *Nat Commun*. 2014;5:5694.
13 Lim SY, Shklovskaya E, Lee JH, et al. The molecular and functional landscape of resistance to immune checkpoint blockade in melanoma. *Nat Commun*. 2023;14(1):1516.
14 Barbie DA, Tamayo P, Boehm JS, et al. Systematic RNA interference reveals that oncogenic KRAS-driven cancers require TBK1. *Nature*. 2009;462(7269):108–112.
15 Liberzon A, Birger C, Thorvaldsdottir H, Ghandi M, Mesirov JP, Tamayo P. The Molecular Signatures Database (MSigDB) hallmark gene set collection. *Cell Syst*. 2015;1(6):417–425.

16 Hoek KS, Schlegel NC, Brafford P, et al. Metastatic potential of melanomas defined by specific gene expression profiles with no BRAF signature. *Pigment Cell Res*. 2006;19(4):290–302.
17 McCarthy DJ, Campbell KR, Lun AT, Wills QF. Scater: pre-processing, quality control, normalization and visualization of single-cell RNA-seq data in R. *Bioinformatics*. 2017;33(8):1179–1186.
18 Lin Y, Cao Y, Kim HJ, et al. scClassify: sample size estimation and multiscale classification of cells using single and multiple reference. *Mol Syst Biol*. 2020;16(6):e9389.
19 Durante MA, Rodriguez DA, Kurtenbach S, et al. Single-cell analysis reveals new evolutionary complexity in uveal melanoma. *Nat Commun*. 2020;11(1):496.
20 Jerby-Arnon L, Shah P, Cuoco MS, et al. A cancer cell program promotes T cell exclusion and resistance to checkpoint blockade. *Cell*. 2018;175(4):984–997.e24.
21 Gao T, Soldatov R, Sarkar H, et al. Haplotype-aware analysis of somatic copy number variations from single-cell transcriptomes. *Nat Biotechnol*. 2022;41:417–426.
22 Hao Y, Hao S, Andersen-Nissen E, et al. Integrated analysis of multimodal single-cell data. *Cell*. 2021;184(13):3573–3587.e29.
23 Lin Y, Cao Y, Willie E, Patrick E, Yang JYH. Atlas-scale single-cell multi-sample multi-condition data integration using scMerge2. *Nat Commun*. 2023;14(1):4272.
24 Blondel VD, Guillaume J-L, Lambiotte R, Lefebvre E. Fast unfolding of communities in large networks. *J Stat Mech Theor Exp*. 2008;2008(10):P10008.
25 Nazarian R, Shi H, Wang Q, et al. Melanomas acquire resistance to B-RAF(V600E) inhibition by RTK or N-RAS upregulation. *Nature*. 2010;468(7326):973–977.
26 Pratilas CA, Taylor BS, Ye Q, et al. (V600E)BRAF is associated with disabled feedback inhibition of RAF-MEK signaling and elevated transcriptional output of the pathway. *Proc Natl Acad Sci U S A*. 2009;106(11):4519–4524.
27 Kuznetsova A, Brockhoff PB, Christensen RHB. lmerTest package: tests in linear mixed effects models. *J Stat Software*. 2017;82(13):1–26.
28 Korotkevich G, Sukhov V, Budin N, et al. Fast gene set enrichment analysis. *bioRxiv*; 2021. https://doi.org/10.1101/060012.
29 Lin Y, Ghazanfar S, Wang KYX, et al. scMerge leverages factor analysis, stable expression, and pseudoreplication to merge multiple single-cell RNA-seq datasets. *Proc Natl Acad Sci U S A*. 2019;116(20):9775–9784.
30 Pozniak J, Pedri D, Landeloos E, et al. A TCF4-dependent gene regulatory network confers resistance to immunotherapy in melanoma. *Cell*. 2024;187(1):166–183.e25.
31 Zaretsky JM, Garcia-Diaz A, Shin DS, et al. Mutations associated with acquired resistance to PD-1 blockade in melanoma. *N Engl J Med*. 2016;375(9):819–829.
32 Hugo W, Zaretsky JM, Sun L, et al. Genomic and transcriptomic features of response to anti-PD-1 therapy in metastatic melanoma. *Cell*. 2017;168(3):542.
33 Hugo W, Shi H, Sun L, et al. Non-genomic and immune evolution of melanoma acquiring MAPKi resistance. *Cell*. 2015;162(6):1271–1285.
34 Rizos H, Menzies AM, Pupo GM, et al. BRAF inhibitor resistance mechanisms in metastatic melanoma: spectrum and clinical impact. *Clin Cancer Res*. 2014;20(7):1965–1977.
35 Park JJ, Stewart A, Irvine M, et al. Protein kinase inhibitor responses in uveal melanoma reflects a diminished dependency on PKC-MAPK signaling. *Cancer Gene Ther*. 2022;29(10):1384–1393.
36 Park JJ, Hamad SA, Stewart A, Carlino MS, Lim SY, Rizos H. PKC-independent PI3K signalling diminishes PKC inhibitor sensitivity in uveal melanoma. *Oncogenesis*. 2024;13(1):9.
37 Hoek KS, Eichhoff OM, Schlegel NC, et al. In vivo switching of human melanoma cells between proliferative and invasive states. *Cancer Res*. 2008;68(3):650–656.
38 Lim SY, Alavi S, Ming Z, et al. Melanoma cell state-specific responses to TNFalpha. *Biomedicines*. 2021;9(6):605.
39 Kim YJ, Sheu KM, Tsoi J, et al. Melanoma dedifferentiation induced by IFN-gamma epigenetic remodeling in response to anti-PD-1 therapy. *J Clin Invest*. 2021;131(12):e145859.
40 Ascierto PA, Mandala M, Ferrucci PF, et al. Sequencing of ipilimumab plus nivolumab and encorafenib plus binimetinib for untreated BRAF-mutated metastatic melanoma (SECOMBIT): a Randomized, three-Arm, open-label phase II trial. *J Clin Oncol*. 2023;41(2):212–221.
41 Long GV, Arance A, Mortier L, et al. Antitumor activity of ipilimumab or BRAF +/- MEK inhibition after pembrolizumab treatment in patients with advanced melanoma: analysis from KEYNOTE-006. *Ann Oncol*. 2022;33(2):204–215.
42 Atkins MB, Lee SJ, Chmielowski B, et al. Combination dabrafenib and trametinib versus combination nivolumab and ipilimumab for patients with advanced BRAF-mutant melanoma: the DREAMseq Trial - ECOG-ACRIN EA6134. *J Clin Oncol*. 2023;41(2):186–197.
43 Harbst K, Staaf J, Lauss M, et al. Molecular profiling reveals low- and high-grade forms of primary melanoma. *Clin Cancer Res*. 2012;18(15):4026–4036.
44 Lim SY, Lee JH, Gide TN, et al. Circulating cytokines predict immune-related toxicity in melanoma patients receiving anti-PD-1-based immunotherapy. *Clin Cancer Res*. 2019;25(5):1557–1563.
45 Wilmott JS, Haydu LE, Menzies AM, et al. Dynamics of chemokine, cytokine, and growth factor serum levels in BRAF-mutant melanoma patients during BRAF inhibitor treatment. *J Immunol*. 2014;192(5):2505–2513.
46 Laino AS, Woods D, Vassallo M, et al. Serum interleukin-6 and C-reactive protein are associated with survival in melanoma patients receiving immune checkpoint inhibition. *J Immunother Cancer*. 2020;8(1):e000842.
47 Konieczkowski DJ, Johannessen CM, Abudayyeh O, et al. A melanoma cell state distinction influences sensitivity to MAPK pathway inhibitors. *Cancer Discov*. 2014;4(7):816–827.
48 Smith MP, Sanchez-Laorden B, O'Brien K, et al. The immune microenvironment confers resistance to MAPK pathway inhibitors through macrophage-derived TNFalpha. *Cancer Discov*. 2014;4(10):1214–1229.